Inorganic Chemistry
Cite This: Inorg. Chem. XXXX, XXX, XXX−XXX
Article
pubs.acs.org/IC

Effects of Lewis Acidic Metal Ions (M) on Oxygen-Atom Transfer Reactivity of Heterometallic Mn_3MO_4 Cubane and $Fe_3MO(OH)$ and $Mn_3MO(OH)$ Clusters

Davide Lionetti,[†] Sandy Suseno,[†] Emily Y. Tsui,[†] Luo Lu,[§] Troy A. Stich,[§] Kurtis M. Carsch,[†,‡] Robert J. Nielsen,[†,‡] William A. Goddard, III,[†,‡] R. David Britt,[§] and Theodor Agapie*[,†]

[†]Division of Chemistry and Chemical Engineering and [‡]Materials and Process Simulation Center, California Institute of Technology, Pasadena, California 91125, United States

[§]Department of Chemistry, University of California, Davis, California 95616, United States

Supporting Information

ABSTRACT: The modulation of the reactivity of metal oxo species by redox inactive metals has attracted much interest due to the observation of redox inactive metal effects on processes involving electron transfer both in nature (the oxygen-evolving complex of Photosystem II) and in heterogeneous catalysis (mixed-metal oxides). Studies of small-molecule models of these systems have revealed numerous instances of effects of redox inactive metals on electron- and group-transfer reactivity. However, the heterometallic species directly involved in these transformations have rarely been structurally characterized and are often generated *in situ*. We have previously reported the preparation and structural characterization of multiple series of heterometallic clusters based on Mn_3 and Fe_3 cores and described the effects of Lewis acidity of the heterometal incorporated in these complexes on cluster reduction potential. To determine the effects of Lewis acidity of redox inactive metals on group transfer reactivity in structurally well-defined complexes, we studied $[Mn_3MO_4]$, $[Mn_3MO(OH)]$, and $[Fe_3MO(OH)]$ clusters in oxygen atom transfer (OAT) reactions with phosphine substrates. The qualitative rate of OAT correlates with the Lewis acidity of the redox inactive metal, confirming that Lewis acidic metal centers can affect the chemical reactivity of metal oxo species by modulating cluster electronics.

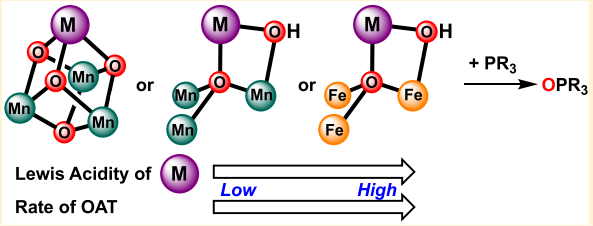

1. INTRODUCTION

Lewis acidic, redox inactive metal ions are known to influence electron- and group-transfer processes in both natural and synthetic systems.[1−3] In biology, the preeminent example is that of the redox inactive Ca^{2+} center found in the oxygen evolving complex (OEC) of Photosystem II (PSII), a Mn_4CaO_x cluster responsible for water oxidation to dioxygen in plants, algae, and cyanobacteria. Although its role has not been fully elucidated, Ca^{2+} is an essential cofactor in this system.[4,5] Redox inactive metals likewise affect the catalytic behavior of heterogeneous mixed-metal oxides in reactions such as water oxidation and dioxygen reduction.[6−8] The reactivity of inorganic oxidants (e.g., MnO_4^-, $Cr_2O_7^{2-}$) with organic substrates can be modulated by Lewis acidic additives.[9−15] Redox inactive metals have been reported to affect the rate of phosphine oxygenation by a Mn^V−oxo complex.[16] Lewis acidic, redox inactive metal ions show a range of effects on the oxygen atom transfer (OAT) reactivity of high-valent Fe−, Mn−, and Co−oxo species including rate enhancement and shifts in reaction mechanism.[17−25] Lewis acid induced O−O bond cleavage or release of O_2 from a Fe(III)-bound peroxide species has also been reported.[26,27] The effects of Lewis acids on group transfer reactions by high-valent Mn, Fe, and V complexes, including those under catalytic conditions, have been described.[28−33] Sc^{3+} has been reported to affect the formation and reactivity of Fe(III)−(hydro) peroxo species.[34,35] While the observation of substantial effects of redox inactive metals on oxygen related redox chemistry is well-demonstrated, structural characterization of the precursor Lewis acid bound species active in these transformations remains a challenge. In most cases, reactive species are generated *in situ* by addition of large excesses of Lewis acid additives to high-valent metal oxo complexes. Although spectroscopic studies of the interaction of metal oxo complexes with metal ions in solution have been described in select cases, structural characterization of these species has rarely been reported.[17,36] The only crystallographically characterized high-valent metal oxo/redox inactive metal ion adduct, a $[Fe(IV)−O−Sc^{3+}]$ complex,[17] has recently been reassigned as a $[Fe(III)−(OH)−Sc^{3+}]$ species based on spectroscopic characterization and structural comparisons with other Fe(III) and Fe(IV) complexes.[37,38] Therefore, conclusions drawn from the majority of these studies must account for both the effect of Lewis acid binding to metal−oxo species

Received: September 21, 2018

DOI: 10.1021/acs.inorgchem.8b02701
Inorg. Chem. XXXX, XXX, XXX−XXX

and for the dynamic equilibrium processes responsible for these interactions.

Incorporation of Lewis acidic metal centers in well-defined multimetallic complexes precludes the need for use of excess Lewis acid additives by providing structurally unambiguous precursors for reactivity studies. This is an appealing strategy for such studies, as it enables a less ambiguous interpretation of any observed heterometallic effects on reactivity. Recently, studies of the effect of redox inactive additives on reactivity related to oxygen or atom-transfer processes[44−48] and on photocatalytic water oxidation[49] have been reported. Our group has studied the effects of Lewis acidity of a redox inactive metal center on the reduction potential of well-defined heterometallic clusters.[3,39−43] Tetrametallic complexes were supported by a multinucleating ligand framework and contained a Mn_3 or Fe_3 core, as well as a fourth, redox inactive metal (M). Tetraoxo $[Mn_3MO_4]$ cubane clusters, as well as oxo-hydroxo $[Mn_3MO(OH)]$ (previously assigned as $[Mn_3MO_2]$ dioxo species, *vide infra*) and $[Fe_3MO(OH)]$ clusters were investigated. A linear correlation was discovered between the Lewis acidity of the redox inactive metal and the reduction potential of the cluster,[40,42,43] supporting the plausibility of a potential-tuning role for redox inactive metals in biological and heterogeneous systems. Although comparisons of these complexes have focused on their one-electron reduction potentials (a thermodynamic parameter), these clusters are well-suited to further exploration of the effects of redox inactive metals on chemical reactivity. We have previously reported initial studies of reactions of cubane clusters with phosphines,[50] including investigations into the mechanism of OAT from these species. However, an extensive structure−function study involving a broader range of cluster structures containing redox-inactive metals of varying Lewis acidity has not previously been carried out. Importantly, our structurally characterized heterotetrametallic clusters provide well-defined precursors for OAT reactions, and the availability of structurally analogous complexes containing different redox inactive metals allows for direct comparison of their effects. Herein, we describe the qualitative assessment of OAT reactivity with phosphine substrates (Scheme 1) of three

Scheme 1. Oxidation of Phosphines Investigated in the Present Study

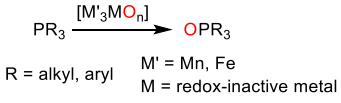

series of complexes: $[Mn_3MO_4]$ cubanes and $[Mn_3MO(OH)]$, and $[Fe_3MO(OH)]$ oxo-hydroxo complexes. The reassignment of Mn_3 oxo-hydroxo clusters, previously identified as the corresponding $[Mn_3MO_2]$ dioxo complexes, on the basis of spectroscopic and computational data is also discussed.

2. RESULTS AND DISCUSSION

2.1. OAT Reactivity of $[Mn_3MO_4]$ Cubanes (M = Ca^{2+}, Gd^{3+}, Sc^{3+}, Mn^{3+}). The OAT reactivity of $[Mn^{IV}_3CaO_4]$, $[Mn^{IV}_3ScO_4]$, and $[Mn^{III}_2Mn^{IV}_2O_4]$ (Figure 1) with trialkylphosphines has previously been described.[50] Reaction of $[Mn^{III}_2Mn^{IV}_2O_4]$ with trimethylphosphine (PMe_3, 2 equiv) led to rapid generation of trioxo cluster $[Mn^{III}_4O_3]$, in which the bottom oxide ligand is absent (Scheme 2). Cubane complex $[Mn^{IV}_3CaO_4]$ was instead found to be unreactive toward PMe_3. This observation is consistent with the greater oxidizing power of $[Mn^{III}_2Mn^{IV}_2O_4]$ as indicated by its more positive one-electron reduction potential ($E_{1/2}$ = −0.70 vs −0.94 V vs $Fc^{+/0}$ for $[Mn^{IV}_3CaO_4]$). In contrast with this model, $[Mn^{IV}_3ScO_4]$ displayed only slow reactivity with PMe_3, generating an intractable mixture of metal-containing products, despite being a stronger oxidant than $[Mn^{III}_2Mn^{IV}_2O_4]$ ($E_{1/2}$ = −0.24 vs −0.70 V vs $Fc^{+/0}$, respectively; see Table 1).

These seemingly contradictory observations can be rationalized by considering the previously studied mechanism of transfer of an oxygen atom from the cubane cluster to PMe_3. According to earlier computations,[50] OAT involving cubane clusters $[Mn^{IV}_3MO_4]$ and $[Mn^{III}Mn^{IV}_2MO_4]$ proceeds via initial dissociation of a bridging acetate ligand from one of the three core Mn centers. The Mn^{III} center (high spin, d^4) in complexes $[Mn^{III}Mn^{IV}_2MO_4]$ is more substitutionally labile due to electrons occupying a Mn−O σ−antibonding orbital. Thus, metal−carboxylate interactions in complexes $[Mn^{III}Mn^{IV}_2MO_4]$ are weaker than in the case of $[Mn^{IV}_3MO_4]$ clusters, in which all Mn centers are in the Mn^{IV} oxidation state (d^3). The difference in Mn oxidation states between $[Mn^{IV}_3MO_4]$ and $[Mn^{III}Mn^{IV}_2MO_4]$ affects the kinetics of ligand dissociation, and only indirectly the OAT process, resulting in slower reactivity of $[Mn^{IV}_3ScO_4]$ despite a larger driving force for electron transfer.

On the basis of this interpretation, it was thus postulated that one-electron reduction of other $[Mn^{IV}_3MO_4]$ clusters, resulting in generation of a kinetically labile Mn^{III} center, would provide more reactive precursors for OAT reactivity, enabling more extensive comparisons of the effects of redox inactive metal of varying Lewis acidity on this transformation. One-electron reduction of $[Mn^{IV}_3MO_4]$ complexes was achieved using cobaltocene ($CoCp_2$) or decamethylferrocene ($FeCp^*_2$) as reductant. Reduction of $[Mn^{IV}_3CaO_4]$ with $CoCp_2$ generated a highly unstable material, which could not be isolated cleanly, and was therefore not investigated further. Reduction of $[Mn^{IV}_3ScO_4]$ and $[Mn^{IV}_3GdO_4]$, however, successfully yielded corresponding $[Mn^{III}Mn^{IV}_2ScO_4]$ and $[Mn^{III}Mn^{IV}_2GdO_4]$ clusters as reported previously.[39,40] Treatment of $[Mn^{III}Mn^{IV}_2ScO_4]$, with PMe_3 (10 equiv) results in clean conversion to a new species over 1.5 weeks at room temperature as determined by proton nuclear magnetic resonance (^{1}H NMR, Figure S6). The reaction could be accelerated by heating to 50 °C in benzene, resulting in full conversion to the same product in 35 h (Figure S7). As a control, heating of $[Mn^{III}Mn^{IV}_2ScO_4]$ in the absence of PMe_3 led to negligible (<10%) conversion. The product of reaction of $[Mn^{III}Mn^{IV}_2ScO_4]$ with PMe_3 was characterized by single-crystal X-ray diffraction (XRD) as the trioxo complex $[Mn^{III}_3ScO_3]$ (Figure 2), analogous to the previously reported reaction of $[Mn^{III}_2Mn^{IV}_2O_4]$ to generate $[Mn^{III}_4O_3]$.[50] The average Mn−oxo and Mn−O(acetate) distances in $[Mn^{III}_3ScO_3]$ are 1.88 and 2.10 Å, respectively, consistent with the assignment of the Mn_3 core as $[Mn^{III}]_3$. No signal for trimethylphophine oxide ($OPMe_3$), the expected byproduct of OAT, was detected by ^{31}P NMR spectroscopy during the reaction. The $OPMe_3$ generated in the reaction is thus proposed to be bound to the nascent $[Mn^{III}_3ScO_3]$, at least in solution under the reaction conditions. Formation of $OPMe_3$ was however confirmed at the end of the reaction via gas chromatography mass-spectrometry (GC-MS) following work-up that included removal of unreacted, volatile PMe_3 (see the Experimental Section).

DOI: 10.1021/acs.inorgchem.8b02701
Inorg. Chem. XXXX, XXX, XXX−XXX

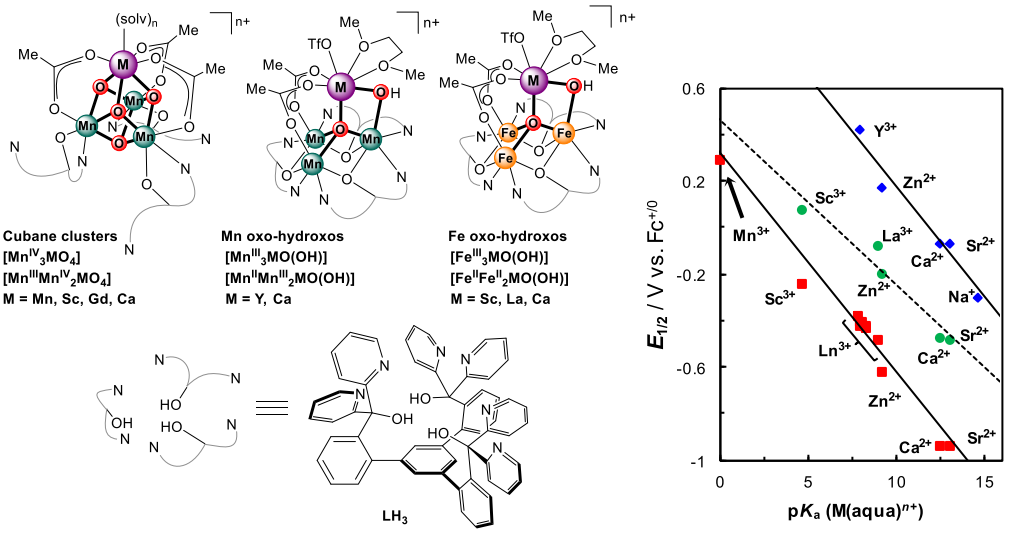

Figure 1. Left: Heterotetrametallic clusters investigated for OAT reactivity. Right: plots of cluster redox potentials vs pK_a of M(aqua)$^{n+}$ ion (as measure of Lewis acidity) summarizing the previously reported redox inactive metal effects on redox processes of heterometallic clusters (red squares: [Mn_3MO_4] cubane clusters;[39−41] green circles: [$Fe_3MO(OH)$] oxo-hydroxo clusters;[42] blue diamonds: [$Mn_3MO(OH)$] oxo-hydroxo clusters,[43] *vide infra*; the red square labeled as "Mn^{3+}" corresponds to the [$Mn^{III}Mn^{IV}_3$]/[$Mn^{III}_2Mn^{IV}_2$] couple in the all-manganese cubane cluster).[41]

Scheme 2. OAT Reactivity of [Mn_3MO_4] Cubane Clusters

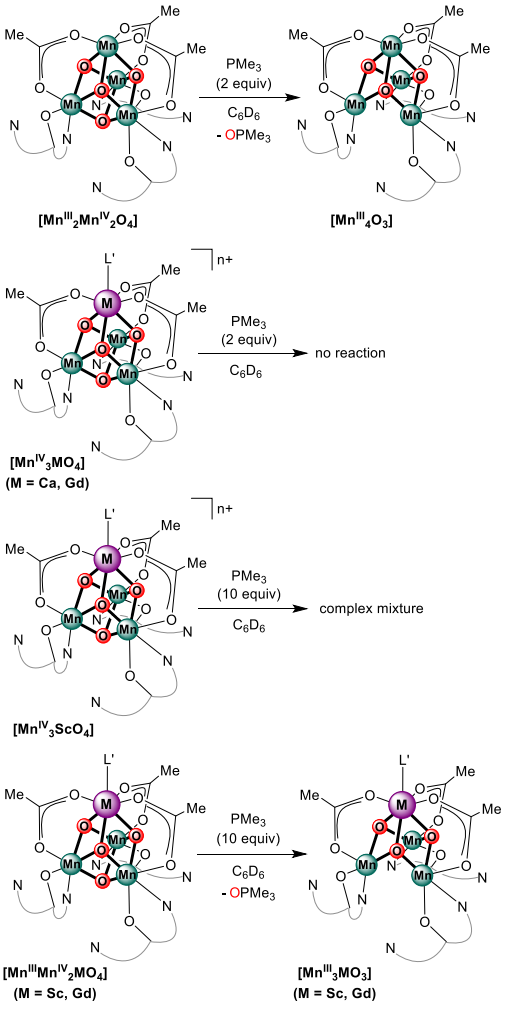

Treatment of [$Mn^{III}Mn^{IV}_2GdO_4$], containing a significantly less Lewis acidic Gd^{3+} center (pK_a = 8.4 for Gd^{3+} vs 4.8 for Sc^{3+}) with PMe_3 (10 equiv) at 50 °C in benzene led to complete conversion of the starting material over 50 h to a stable new product (heating in the absence of PMe_3 did not lead to detectable conversion). Although crystallographic characterization of this product was unsuccessful, this species was assigned as the trioxo cluster [$Mn^{III}_3GdO_3$] on the basis of the similarity of its ^{1}H NMR features with those for structurally characterized [$Mn^{III}_3ScO_3$] (Figure S8). As a signal for $OPMe_3$ was detected during the reaction by ^{31}P NMR, the reaction was monitored by NMR spectroscopy upon treating [$Mn^{III}Mn^{IV}_2ScO_4$] with a smaller excess of PMe_3 (3 equiv) at 50 °C to improve accuracy of integration of NMR signal. This experiment was performed in the presence of PPh_3 (2 equiv) as an internal standard. A total of 1 equiv of PMe_3 was consumed throughout the reaction (67 h), and formation of the same metal species was observed (^{1}H NMR, Figure S9). The reaction stoichiometry (1:1 [$Mn^{III}Mn^{IV}_2GdO_4$]/PMe_3) is

Table 1. One-Electron Redox Potentials of Selected [$Mn^{IV}_3MO_4$] and [$Mn^{III}Mn^{IV}_2MO_4$] Clusters

compound	$E_{1/2}$ (V vs $Fc^{+/0}$)	redox couple
[$Mn^{III}_2Mn^{IV}_2O_4$][41]	−0.70	$Mn^{III}_2Mn^{IV}_2/Mn^{III}_3Mn^{IV}$
[$Mn^{IV}_3CaO_4$][41]	−0.94	$MMn^{IV}_3/MMn^{III}Mn^{IV}_2$
[$Mn^{IV}_3ScO_4$][40]	−0.24	$MMn^{IV}_3/MMn^{III}Mn^{IV}_2$

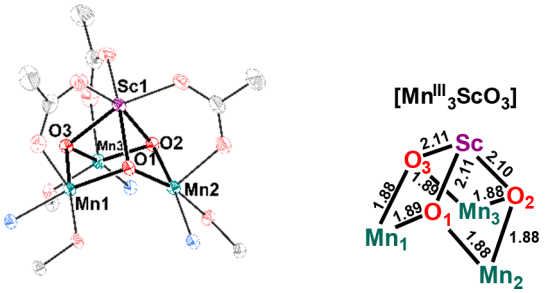

Figure 2. Left: truncated solid-state structure of [$Mn^{III}_3ScO_3$]. Right: relevant M−O and Mn−O bond distances in Å.

DOI: 10.1021/acs.inorgchem.8b02701
Inorg. Chem. XXXX, XXX, XXX−XXX

Table 2. Summary of OAT Reactivity of Heterometallic Mn_3 and Fe_3 Clusters

entry	compound	$E_{1/2}$ (vs $Fc^{+/0}$)[a]	Lewis acid	pK_a[51]	substrate (equiv)	time[b]	T (°C)
1[37]	$[Mn^{IV}_3ScO_4]$	−0.24 V[40]	Sc^{3+}	4.8	PMe_3 (2)	N.R.	r.t.
2[37]	$[Mn^{IV}_3CaO_4]$	−0.94 V[41]	Ca^{2+}	12.9	PMe_3 (2)	N.R.	r.t.
3	$[Mn^{III}_2Mn^{IV}_2O_4]$	−0.70 V[41]	Mn^{3+}	0.1	PMe_3 (2)	15 min	r.t.
4	$[Mn^{III}Mn^{IV}_2ScO_4]$		Sc^{3+}	4.8	PMe_3 (10)	1.5 weeks	r.t.
5	$[Mn^{III}Mn^{IV}_2ScO_4]$		Sc^{3+}	4.8	PMe_3 (10)	35 h	50 °C
6	$[Mn^{III}Mn^{IV}_2GdO_4]$		Gd^{3+}	8.4	PMe_3 (10)	>2 weeks	r.t.
7	$[Mn^{III}Mn^{IV}_2GdO_4]$		Gd^{3+}	8.4	PMe_3 (10)	50 h	50 °C
8	$[Mn^{III}_3YO(OH)]_2$	+0.42 V[43]	Y^{3+}	8.6	PEt_3 (10)	15 min	r.t.
9	$[Mn^{III}_3YO(OH)]_2$	+0.42 V[43]	Y^{3+}	8.6	PPh_3 (10)	30 min	r.t.
10	$[Mn^{III}_3CaO(OH)]$	−0.07 V[43]	Ca^{2+}	12.9	PEt_3 (10)	3 h	r.t.
11	$[Mn^{III}_3CaO(OH)]$	−0.07 V[43]	Ca^{2+}	12.9	PPh_3 (10)	20 h	r.t.
12	$[Mn^{II}Mn^{III}_2YO(OH)]$		Y^{3+}	8.6	PEt_3 (10)	30 min	r.t.
13	$[Mn^{II}Mn^{III}_2YO(OH)]$		Y^{3+}	8.6	PPh_3 (10)	1 h	r.t.
14	$[Mn^{II}Mn^{III}_2CaO(OH)]$		Ca^{2+}	12.9	PEt_3 (10)	36 h	r.t.
15	$[Mn^{II}Mn^{III}_2CaO(OH)]$		Ca^{2+}	12.9	PPh_3 (10)	>2 weeks	r.t.
16	$[Fe^{III}_3LaO(OH)]$	−0.08 V[42]	La^{3+}	9.06	PPh_3 (10)	24 h	r.t.
17	$[Fe^{III}_3CaO(OH)]$	−0.48 V[42]	Ca^{2+}	12.9	PPh_3 (10)	N.R.	r.t.
18	$[Fe^{II}Fe^{III}_2ScO(OH)]$		Sc^{3+}	4.8	PMe_3 (10)	14 h	r.t.
19	$[Fe^{II}Fe^{III}_2LaO(OH)]$		La^{3+}	9.06	PMe_3 (10)	130 h	r.t.
20	$[Fe^{II}Fe^{III}_2CaO(OH)]$		Ca^{2+}	12.9	PMe_3 (10)	270 h	r.t.

[a] $Fc^{+/0}$ = ferrocenium/ferrocene couple; only potentials for relevant reduction events included. [b] N.R. = no reaction observed.

consistent with transfer of a single O atom equivalent during the reaction, corroborating the assignment of the metal-containing product as trioxo species $[Mn^{III}_3GdO_3]$. Notably, $[Mn^{III}_3GdO_3]$ is stable even in the presence of a large excess of PMe_3 (10 equiv), and formation of reduced clusters with <3 oxide ligands, the products of further OAT processes, was not observed.

The observed rate of OAT from $[Mn^{III}Mn^{IV}_2MO_4]$ clusters to phosphine substrates correlates with the Lewis acidity of M (Table 2, entries 1−7). To generate these correlations, we have used the pK_a of the $M(H_2O)_n$ ion[51] as a measure of Lewis acidity; in our previous work, this scale of Lewis acidity has enabled analogous correlations between Lewis acidity and reduction potential. Analysis of the qualitative, relative rates of OAT of $[Mn^{III}Mn^{IV}_2MO_4]$ complexes with PMe_3 as substrate yields the following trend: $[Mn^{III}_2Mn^{IV}_2O_4] > [Mn^{III}Mn^{IV}_2ScO_4] > [Mn^{III}Mn^{IV}_2GdO_4]$.

The decrease in OAT rate correlates with the progressively higher pK_a (i.e., lower Lewis acidity) across this series of metals ($pK_a(M(H_2O)_n)$: Mn^{3+} = 0.1, Sc^{3+} = 4.7, Gd^{3+} = 8.4).[51] Most notably, changing from Mn to Gd results in decrease in the rate of OAT by more than 3 orders of magnitude.

2.2. Structural Reassignment of $[Mn_3MO_2(H)]$ Clusters (M = Na^+, Sr^{2+}, Ca^{2+}, Zn^{2+}, Y^{3+}). Comparisons of the structural parameters between initially reported Mn_3MO_2 clusters and more recently prepared $Fe_3MO(OH)$ show strong similarities. Through a combination of EPR, XRD, and computational studies, these Mn clusters were reassigned as $Mn_3MO(OH)$, with an oxidation state of $[Mn^{III}_3MO(OH)]$ as $[Mn^{III}_3]$ and of $[Mn^{II}Mn^{III}_2MO(OH)]$ as $[Mn^{III}_2Mn^{II}]$. A detailed discussion of these data and their interpretation is presented in Supporting Information, page S3. It should be noted that the changes in assignment of the oxidation states and identity of bridging ligands in clusters $[Mn^{III}_3MO(OH)]$ and $[Mn^{II}Mn^{III}_2MO(OH)]$ bear no effect on the conclusions of earlier studies on these complexes regarding the effect of the redox inactive metal on reduction potentials.[43] All comparisons within this series of complexes remain valid, as changes affect compounds across the entire series. The reactivity studies described next were focused on the available oxo-hydroxo complexes.

2.3. OAT Reactivity of $[Mn_3MO(OH)]$ Clusters (M = Ca^{2+}, Y^{3+}). OAT reactivity of complexes $[Mn^{III}_3MO(OH)]$ and $[Mn^{II}Mn^{III}_2MO(OH)]$ was investigated using phosphines as substrates (Scheme 3; Table 2, entries 8−15). Clusters

Scheme 3. OAT Reactivity of Mn_3 Oxo-Hydroxo Clusters $[Mn^{III}_3MO(OH)]$ and $[Mn^{II}Mn^{III}_2MO(OH)]$

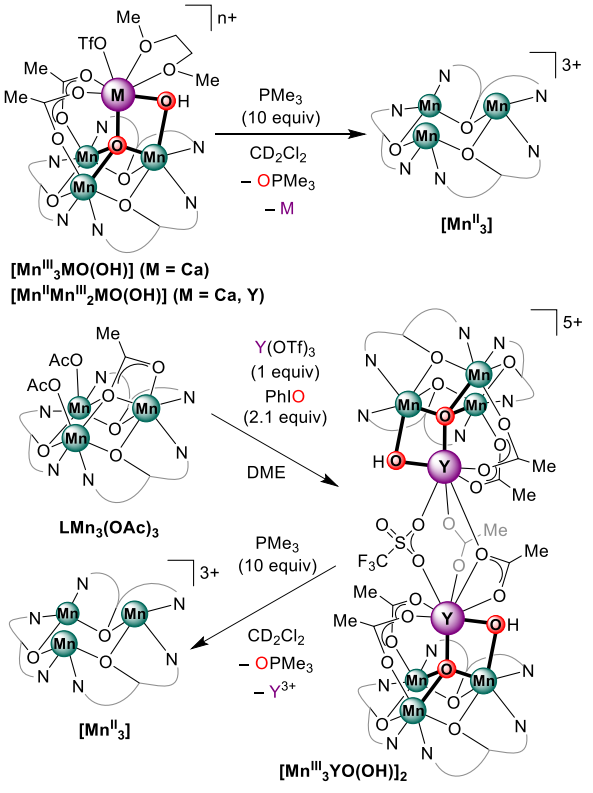

DOI: 10.1021/acs.inorgchem.8b02701
Inorg. Chem. XXXX, XXX, XXX−XXX

$[Mn^{III}_3MO(OH)]$ and $[Mn^{II}Mn^{III}_2MO(OH)]$ displayed faster reactivity with phosphines than that of cubane complexes $[Mn^{IV}_3MO_4]$ and $[Mn^{III}Mn^{IV}_2MO_4]$. Triethylphosphine (PEt_3) and triphenylphosphine (PPh_3) were used, as PMe_3 resulted in reactivity too rapid for comparisons to be possible by ^{1}H NMR spectroscopy. Treatment of $[Mn^{II}Mn^{III}_2CaO(OH)]$ with 10 equiv of PEt_3 led to conversion, over 36 h, to a product with very broad ^{1}H NMR features (Figure S16), typical of $[LMn^{II}_3X_3]$ (X = $^-$OAc or $^-$OTf) species.[52] This observation is consistent with loss of the redox inactive metal center following OAT. Similar to the case of cubane clusters, triethylphosphine oxide ($OPEt_3$), the product substrate oxidation, was not observed spectroscopically during the reaction. Removal of solvents and excess PEt_3 *in vacuo* after completion, followed by methanolysis and analysis by GC-MS allowed for identification of the $OPEt_3$ product. $[Mn^{II}Mn^{III}_2CaO(OH)]$ also reacts with the weaker O-atom acceptor PPh_3, albeit much more slowly (>2 weeks; Figure S17).

As expected, the more oxidized cluster $[Mn^{III}_3CaO(OH)]$ reacts more rapidly with both PEt_3 and PPh_3; full conversion was achieved in 3 and 20 h, respectively (Figures S12 and S13). Similar to $[Mn^{II}Mn^{III}_2CaO(OH)]$, OAT from $[Mn^{III}_3CaO(OH)]$ results in formation of reduced Mn^{II}_3 species whose structural characterization was unsuccessful. Clusters displaying the more Lewis acidic Y^{3+} ion yield faster reactivity. Reaction of $[Mn^{II}Mn^{III}_2YO(OH)]$ with PEt_3 (10 equiv) proceeded to completion in 30 min (Figure S14), whereas reaction with PPh_3 was complete in 1 h (Figure S15). As before, generation of Mn^{II}_3 species was suggested by the broad ^{1}H NMR features observed. Although isolation of monomeric oxidized complex $[Mn^{III}_3YO(OH)]$ has not been achieved to date via either direct synthesis or transmetalation from $[Mn^{III}_3CaO(OH)]$, a dimeric form of this complex, $[Mn^{III}_3YO(OH)]_2$, has been prepared from precursor complex $LMn_3(OAc)_3$ (^{1}H NMR, elemental analysis). XRD studies have only yielded a poor-quality structure (Figure 3), which is nonetheless sufficient for basic connectivity determination. In this complex, two $[Mn_3YO(OH)]$ cores are bridged by two $^-$OAc and one $^-$OTf ligands, with five outersphere triflate counteranions. $[Mn^{III}_3YO(OH)]_2$ reacts rapidly with phosphine substrates: reaction with PEt_3 (10 equiv/Y) was complete in less than 15 min (Figure S10), and even the more electron-deficient PPh_3 led to complete reaction in 30 min (Figure S11).

Qualitative analysis of the relative OAT rates for clusters $[Mn^{III}_3MO(OH)]$ and $[Mn^{II}Mn^{III}_2MO(OH)]$ reveals the following trend: $[Mn^{III}_3YO(OH)]_2$ > $[Mn^{II}Mn^{III}_2YO(OH)]$ > $[Mn^{III}_3CaO(OH)]$ > $[Mn^{II}Mn^{III}_2CaO(OH)]$.

As observed for the cubane clusters, the complexes containing more Lewis acidic Y^{3+} (pK_a = 8.6) undergo faster OAT processes than those containing Ca^{2+} (pK_a = 12.9), in some case by more than 2 orders of magnitude.[51] Unlike their cubane analogues, which displayed clean transfer of a single oxygen atom to give trioxo clusters, oxo-hydroxo complexes appear to transfer both oxygen atom equivalents to yield $[Mn^{II}_3]$ species. It is probable the first OAT event (presumably on the more sterically accessible μ_2-bridge) relieves steric congestion in the cluster, increasing flexibility and allowing access to the second O-atom. Deprotonation of the hydroxide may precede OAT, though independent deprotonation studies were inconclusive. Formation of mono-oxo complexes en route to the $[Mn^{II}_3]$ products is supported by the observation of

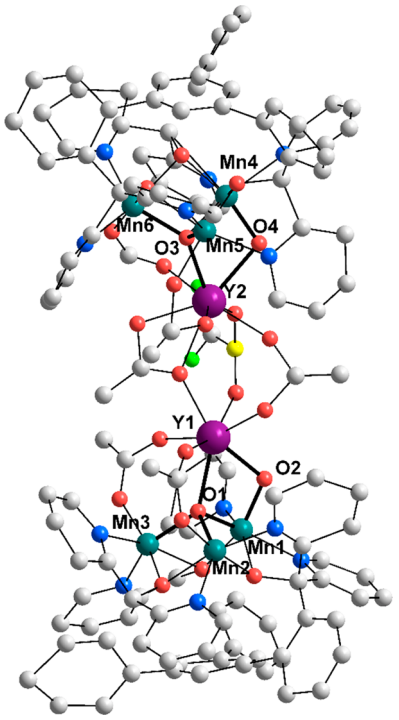

Figure 3. Solid-state structure of $[Mn^{III}_3YO(OH)]_2$. Five molecules of outer sphere triflate anions and hydrogen atoms are omitted for clarity.

intermediate species during the reaction of $[Mn^{II}Mn^{III}_2YO(OH)]$ with PPh_3. After 30 min, ^{1}H NMR features consistent with formation of a $[Mn_3MO]$ species were detected (Figure S3),[41] leading to the proposed generation of tetrametallic monooxo species from $[Mn^{III}_3MO(OH)]$ and $[Mn^{II}Mn^{III}_2MO(OH)]$ clusters prior to the second OAT event and formation of the fully reduced products. Although quantification of the phosphine oxide produced in these processes was attempted *in situ* (^{31}P NMR) as well as following workup (see the Experimental Section for the workup protocol), these procedures led to incomplete accounting of phosphine oxide product even in most cases where the stoichiometry of the reaction was well-established (e.g., the reactivity of cubane clusters $[Mn^{III}Mn^{IV}_2MO_4]$), likely due to strong interaction of the phosphine oxide product with metal-containing byproducts. Thus, the stoichiometry of the reaction of Mn oxo-hydroxo clusters $[Mn^{III}_3MO(OH)]$ and $[Mn^{II}Mn^{III}_2MO(OH)]$ (or their Fe counterparts, *vide infra*) could not be conclusively assigned, except in the case of $[Mn^{III}Mn^{IV}_2ScO_4]$ which reacted to generate cleanly 1 equiv of $(O)PMe_3$ (^{31}P NMR).

2.4. OAT Reactivity of $[Fe_3MO(OH)]$ Clusters (M = Ca^{2+}, La^{3+}, Sc^{3+}). Studies of the OAT reactivity of clusters $[Fe^{III}_3MO(OH)]$ and $[Fe^{II}Fe^{III}_2MO(OH)]$, isostructural to Mn-containing complexes $[Mn^{III}_3MO(OH)]$ and $[Mn^{II}Mn^{III}_2MO(OH)]$, respectively, were carried out with phosphine substrates in an analogous manner to those of cubane and oxo-hydroxo Mn_3 clusters (Scheme 4; Table 2, entries 16–20). Treatment of clusters $[Fe^{III}_3MO(OH)]$, containing three Fe^{III} centers, with electron-rich phosphines such as PMe_3 yielded complex mixtures. Therefore, OAT behavior of $[Fe^{III}_3MO(OH)]$ complexes was investigated with the more electron deficient substrate PPh_3. $[Fe^{III}_3CaO(OH)]$ displays minimal conversion in the presence of PPh_3 (10 equiv,

DOI: 10.1021/acs.inorgchem.8b02701
Inorg. Chem. XXXX, XXX, XXX−XXX

Scheme 4. OAT Reactivity of Fe_3 Oxo-Hydroxo Clusters $[Fe^{III}_3MO(OH)]$ and $[Fe^{II}Fe^{III}_2MO(OH)]$

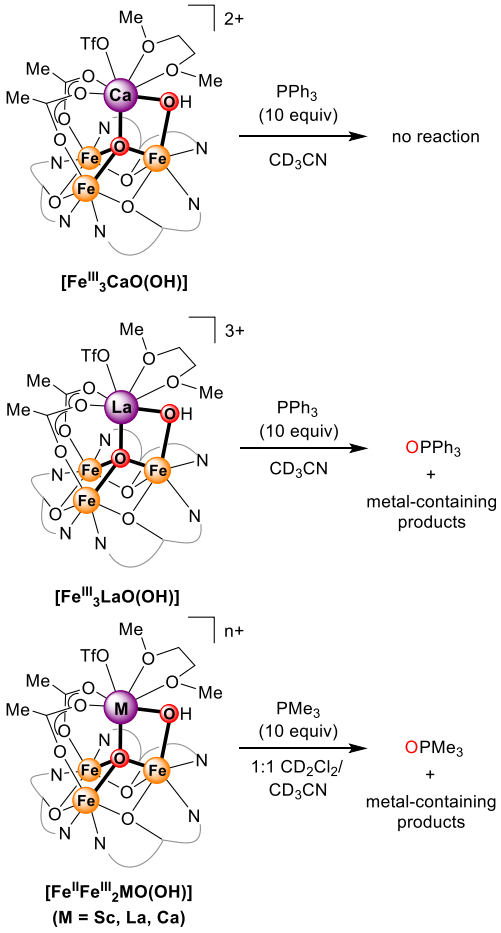

Figure S19). Conversely, $[Fe^{III}_3LaO(OH)]$ reacts completely with PPh_3 (10 equiv) over 14 h, generating $OPPh_3$ as determined via ^{31}P NMR (Figure S18). OAT reactivity of reduced clusters $[Fe^{II}Fe^{III}_2MO(OH)]$ was studied using PMe_3 as substrate. In the presence of a 10-fold excess of PMe_3, $[Fe^{II}Fe^{III}_2ScO(OH)]$ displayed complete conversion in 60 h, slower than that for the more oxidized clusters. The $OPMe_3$ product generated was observed during the reaction via ^{31}P NMR (Figure S20). Treatment of clusters $[Fe^{II}Fe^{III}_2LaO(OH)]$ and $[Fe^{II}Fe^{III}_2CaO(OH)]$ with 10 equiv of PMe_3 resulted in slower reactivity, with full conversion in 130 and 270 h, respectively. As in the case with $[Fe^{II}Fe^{III}_2ScO(OH)]$, generation of $OPMe_3$ was confirmed via ^{31}P NMR as the reaction proceeded (Figure S21 and S22). Unfortunately, characterization of the metal-containing products of these transformations has thus far been unsuccessful. On the basis of the observed reactivity of the Mn_3 analogues $[Mn^{III}_3MO(OH)]$ and $[Mn^{II}Mn^{III}_2MO(OH)]$, it is reasonable to expect that OAT from complexes $[Fe^{III}_3MO(OH)]$ and $[Fe^{II}Fe^{III}_2MO(OH)]$ would also generate mono-oxo complexes as well as reduced Fe^{II}_3 species. However, due to the similarity of the characteristic ^1H NMR features of these families of Fe_3 compounds, deconvolution of the spectroscopic data for the products of OAT has not been successful. Similar to what was observed for Mn_3 complexes, OAT reactivity of Fe_3 oxo-hydroxo complexes $[Fe^{III}_3MO(OH)]$ and $[Fe^{II}Fe^{III}_2MO(OH)]$ is affected by the Lewis acidity of the redox inactive metal. In both oxidation states, the clusters containing the more Lewis acidic heterometal display faster OAT to phosphine substrates. $[Fe^{III}_3CaO(OH)]$ and $[Fe^{II}Fe^{III}_2CaO(OH)]$, containing the least Lewis acidic Ca^{2+} (pK_a = 12.9), react slower than clusters $[Fe^{III}_3LaO(OH)]$ and $[Fe^{II}Fe^{III}_2LaO(OH)]$ and $[Fe^{II}Fe^{III}_2ScO(OH)]$, respectively, which contain stronger Lewis acidic metals (pK_a: La^{3+} = 9.06, Sc^{3+} = 4.8).

2.5. Reactivity Trends. Access to structurally well-defined tetraoxo and oxo-hydroxo clusters displaying both redox active (Mn, Fe) and redox inactive metals has facilitated systematic structure−reactivity studies (Table 2). Although effects of Lewis acidic, redox inactive metals on redox processes such as group transfer reactivity have been previously reported, to our knowledge, this study is the first to employ heterometallic oxo clusters for which an unambiguous structural assignment of the OAT precursors is available. While in previous literature reports redox inactive metal centers were included as additives (often in suprastoichiometric amounts), generating the species responsible for OAT *in situ*, the use of well-defined heterometallic clusters simplifies the interpretation of the observed reactivity. When redox inactive metal additives are used in excess to generate adducts with high-valent metal oxo species *in situ*, the effects of the Lewis acidity on the dynamic equilibria involved in adduct formation must be accounted for when analyzing the reactivity of the proposed adducts. In the present systems, however, the redox inactive metal centers are stoichiometrically incorporated in clusters that can be isolated and structurally characterized. For each type of cluster reported here, the first OAT step is qualitatively faster with increasing Lewis acidity (decreasing pK_a of metal aquo complex) of the redox inactive, apical metal center in the cluster. For oxo-hydroxo complexes, clusters in higher oxidation states display faster OAT reactivity than that of their reduced counterparts. The case of cubane clusters is more complex, as the high kinetic barrier to dissociation of an acetate ligand from the all-Mn^{IV} core in oxidized clusters $[Mn^{IV}_3MO_4]$ inhibits the OAT process (*vide supra*). Notably, in several classes of clusters, the metal-containing species initially generated by the reaction of the well-defined heterometallic precursors with phosphines were observed to themselves undergo further reactivity with phosphines. However, as neither the transiently generated metal-containing species nor the final metal-containing products of these processes could be cleanly isolated, no further information on the reactivity of these systems can be teased out from the available data. Nonetheless, the qualitative analysis of the kinetics of the first step in this reactivity (i.e., the reaction of the well-defined isolated clusters with phosphine substrates) indicates that the choice of Lewis acid plays a significant role in tuning the OAT reactivity of these clusters.

Comparison of the OAT activity of complexes $[Mn^{III}Mn^{IV}_2GdO_4]$, $[Mn^{II}Mn^{III}_2YO(OH)]$, and $[Fe^{II}Fe^{III}_2LaO(OH)]$, which contain heterometals with similar pK_a's (Gd^{3+} = 8.4, Y^{3+} = 8.6, La^{3+} = 9.06), enables assessment of the effect of various cluster architectures on reactivity. Cubane cluster $[Mn^{III}Mn^{IV}_2GdO_4]$ reacts slower (>2 weeks at r.t.) with PMe_3 than $[Fe^{II}Fe^{III}_2LaO(OH)]$ (120 h), which in turn displays slower OAT activity than $[Mn^{II}Mn^{III}_2YO(OH)]$ (30 min, PEt_3). A similar reactivity ordering is observed between clusters containing Ca^{2+} (pK_a = 12.9) as the redox-inactive metal; $[Mn^{II}Mn^{III}_2CaO(OH)]$ reacts faster (36 h) than $[Fe^{II}Fe^{III}_2CaO(OH)]$ (270 h; the corresponding cubane cluster, $[Mn^{III}Mn^{IV}_2CaO_4]$, could not be isolated).

DOI: 10.1021/acs.inorgchem.8b02701
Inorg. Chem. XXXX, XXX, XXX−XXX

The observed qualitative rate of OAT correlates not only with the pK_a of the redox-inactive metal incorporated in the cluster but also with the reported one-electron reduction potentials for the three series of clusters. Fe_3 oxo-hydroxo clusters display overall intermediate potentials in the three series in the present study; the reduction potentials of Fe oxo-hydroxo complexes are typically more positive than those of cubane clusters and more negative than those of Mn oxo-hydroxo complexes (Tables 1 and 2).[40,42,43] In agreement with the electrochemical data, $[Fe_3MO(OH)]$ complexes display slower reactivity than more oxidizing $[Mn_3MO(OH)]$ complexes and in turn undergo faster OAT than the less oxidizing cubane clusters.

The exact mechanism of phosphine oxidation involving electron transfer or concerted O atom transfer[53] cannot be conclusively assigned in all series of clusters based on the available data. The faster OAT observed with clusters displaying more Lewis acidic metals, M, could be a consequence of a more electrophilic oxo motif, or an oxidant that is more prone to undergo single electron transfer. As indicated by computational studies, oxidation of phosphine by cubane clusters $[Mn^{III}Mn^{IV}_2MO_4]$ proceeds via concerted oxygen-atom transfer rather than via electron transfer. This assignment is consistent with the observed slower rate of OAT to the more sterically hindered PEt_3 (vs the less bulky PMe_3 substrate). In the case of oxo-hydroxo clusters $[Mn_3MO(OH)]$ and $[Fe_3MO(OH)]$, however, a stepwise mechanism involving reduction of the cluster species by the PR_3 substrate (i.e., an electron-transfer process) cannot be ruled out.

3. CONCLUSIONS

The Lewis acidity of redox inactive metal centers incorporated in heterometallic Mn_3 and Fe_3 clusters was found to have a substantial effect on the rate of oxygen atom transfer to phosphine substrates. An important feature of these systems is the stoichiometric incorporation a redox-inactive metal center. Moreover, these precursors can be isolated and structurally characterized. Qualitatively, within the same structural motif and redox state, the rate of OAT of cubane $[Mn_3MO_4]$ and oxo-hydroxo $[Mn_3MO(OH)]$ and $[Fe_3MO(OH)]$ clusters correlates with the Lewis acidity of the apical metal, similar to previously observed one-electron reduction potentials of the same series of clusters. OAT rates can be accelerated by between one and 3 orders of magnitude, depending on the nature of the cluster. The more Lewis acidic metals are proposed to increase the electrophilicity of the oxo moieties, promoting OAT. Higher oxidation state clusters further exacerbate this effect, except in the case of all-Mn^{IV} cubane clusters, which display slow ligand dissociation and, consequently, slower OAT. Overall, this study demonstrates that the OAT reactivity of the clusters can be tuned significantly by choice of the Lewis acid.

4. EXPERIMENTAL SECTION

4.1. General Considerations. Unless otherwise specified, all compounds were manipulated using a glovebox or standard Schlenk line techniques with an N_2 atmosphere. Anhydrous tetrahydrofuran (THF) was purchased from Aldrich in 18 L Pure-Pac containers. Anhydrous benzene, dichloromethane, and diethyl ether were purified by sparging with nitrogen for 15 min and then passing under nitrogen pressure through a column of activated A2 alumina (Zapp's). Methylene chloride-d_2 and acetonitrile-d_3 were purchased from Cambridge Isotopes, dried over calcium hydride, and vacuum transferred prior to use. Benzene-d_6 was also purchased from Cambridge Isotope Laboratories, Inc., dried over sodium/benzophenone ketyl, and vacuum transferred prior to use. Unless indicated otherwise, all commercial chemicals were used as received. $LMn_3(OAc)_3$,[52] $[Mn^{IV}_3ScO_4]$,[40] $[Mn^{IV}_3GdO_4]$,[39] $[Mn^{III}Mn^{IV}_2GdO_4]$,[39] $[Mn^{III}_3CaO(OH)]$, $[Mn^{II}Mn^{III}_2YO(OH)]$, $[Mn^{II}Mn^{III}_2CaO(OH)]$,[43] $[Fe^{III}_3LaO(OH)]$, $[Fe^{III}_3CaO(OH)]$, $[Fe^{II}Fe^{III}_2ScO(OH)]$, $[Fe^{II}Fe^{III}_2LaO(OH)]$, and $[Fe^{II}Fe^{III}_2CaO(OH)]$[42] were prepared according to previously published protocols. ^1H and ^{31}P NMR spectra were recorded on a Varian Mercury 300 spectrometer at room temperature. Elemental analyses were performed by Robertson Microlit Laboratories, Ledgewood, NJ.

4.2. Synthesis of $[Mn^{III}_3ScO_3]$. In an inert atmosphere glovebox, $[Mn^{IV}_3ScO_4]$ (13.5 mg, 0.0103 mmol, 1 equiv) was initially dissolved in C_6D_6 in a J. Young NMR tube. To the wall of the J. Young tube was added PMe_3 (11 μL, 0.103 mmol, 10 equiv) quickly via a Hamilton syringe. The J. Young tube was sealed and brought outside the glovebox. The reaction mixture was heated to 50 °C using an oil bath. The reaction was monitored over time by ^1H NMR spectroscopy and was complete after 30 h. The solvent and excess unreacted PMe_3 were removed under vacuum. The residue was washed with Et_2O to remove trace PMe_3. The residue was resuspended in benzene and then filtered. Crystals were obtained via vapor diffusion of Et_2O into a concentrated benzene solution to give the clean product in 56% yield. ^1H NMR (C_6D_6, 300 MHz): δ 17.62 (v br), 10.69 (v br), 9.44 (br overlapped), 9.05 (v br overlapped), 4.57 (br), 3.53 (br), 2.34 (br), 1.84 (br), 1.63 (br), 1.35 (m overlapped), −18.98 (v br) ppm. Anal. Calcd for $C_{63}H_{48}Mn_3N_6O_{12}Sc$ ($[Mn^{III}_3ScO_3]$) (%): C, 58.62; H, 3.75; N, 6.51. Found: C, 57.88; H, 3.70; N, 6.65.

4.3. Synthesis of $[Mn^{III}_3YO(OH)]_2$. To a suspension of $LMn_3(OAc)_3$ (150 mg, 0.125 mmol, 1 equiv) in DME was added $Y(OTf)_3$ (67 mg, 0.125 mmol, 1 equiv). The mixture was stirred for 5 min then PhIO was added (58 mg, 0.263 mmol, 2.1 equiv). The mixture was stirred for 1 h then filtered. The purple filtrate was collected, and the solvent was removed under vacuum. The DME fraction was recrystallized in CH_3CN/Et_2O to give clean product as precipitate in 71% yield. ^1H NMR (CD_2Cl_2, 300 MHz): δ 77.49 (v br), 67.83 (m overlapped), 52.93 (m br overlapped), 41.12 (v br), 38.51 (v br), 35.34 (v br), 25.17 (m br overlapped), 17.40 (br overlapped), 8.3 (m br overlapped),−21.81 (m br overlapped), −24.47 (d br overlapped), −28.05 (m br overlapped), −33.46 (m br overlapped) ppm. Anal. Calcd for $C_{132}H_{96}F_{18}Mn_6N_{12}O_{40}S_6Y_2$ $[Mn^{III}_3YO(OH)]_2$ (%): C, 44.89; H, 2.74; N, 4.76. Found: C, 44.89; H, 2.94; N, 4.57.

4.4. Protocol for Reactivity Studies of Metal-Oxo Clusters with Phosphine Substrate. In an inert-atmosphere glovebox, a J. Young NMR tube was charged with a solution (∼12−15 mM) of the desired cluster complex in an appropriate NMR solvent (CD_2Cl_2, CD_3CN, or C_6D_6). Phosphine (PPh_3, PEt_3, or PMe_3; 2−10 equiv) was added neat via gas-tight microsyringe or as a stock solution in deuterated solvent. Reaction progress was monitored via ^1H and ^{31}P NMR as appropriate until full (>95%) conversion was observed by disappearance of signal corresponding to starting material. Samples requiring heating were kept at elevated temperature in mineral oil baths. When phosphine oxide products were not observed during reaction via ^{31}P NMR, samples were returned to a glovebox, where volatiles were removed *in vacuo*. On the benchtop, the resulting residue was dissolved in dichloromethane, filtered through a short silica plug, and further eluted with methanol. The resulting solution was analyzed by GC-MS to confirm the presence of phosphine oxide product.

4.5. EPR Spectroscopy. Perpendicular-mode continuous-wave (CW) X-Band (9.33−9.37 GHz) spectra were collected using a Bruker E500 spectrometer with a superhigh Q resonator (SHQE). Parallel-mode CW X-Band spectra (9.3 GHz) were collected using a dual-mode cavity (ER 4116DM). All EPR spectra were collected under nonsaturating conditions. Temperature control was maintained with an Oxford Instruments model ESR900 helium-flow cryostat with an Oxford ITC 503 temperature controller and an Oxford Instruments CF935 helium-flow cryostat.

DOI: 10.1021/acs.inorgchem.8b02701
Inorg. Chem. XXXX, XXX, XXX−XXX

4.6. Computational Protocol. Density functional theory (DFT) calculations were carried out on complexes $[LMn^{III}_2Mn^{IV}CaO_2(OTf)(DME)[OTf]_2$ (**oxCa′**), $[LMn^{III}_3CaO(OH)(OTf)(DME)][OTf]_2$ (**oxCa′′**), $[LMn^{III}_3O_2Ca(OTf)(DME)[OTf]$ (**redCa′**), and $[LMn^{II}Mn^{III}_2CaO(OH)(OTf)(DME)][OTf]$ (**redCa′′** and **redCa′′-noH**) to elucidate the structure of complexes $[\mathbf{Mn^{III}_3CaO(OH)}]$ and $[\mathbf{Mn^{II}Mn^{III}_2CaO(OH)}]$. Complexes **oxCa′** and **redCa′** were optimized using the solid-state structure without outer-sphere solvent molecules as the initial geometry input whereas complexes **oxCa′′** and **redCa′′** were modified by placing one triflate in the vicinity (∼3.0 Å) of the bridging hydroxo motif for the initial geometry input. To decrease computational expenses, a "truncated ligand" approximation was employed in which the three carbon atoms connecting the bipyridine motifs were spatially constrained, and the remaining ligand scaffold connecting each carbon atom to the phenyl backbone was substituted with three protons. This approximation is expected not to influence bond parameters for the Mn_3O_2Ca core.

Schrodinger computational products Jaguar 8.4[54] and Maestro were employed respectively to perform gas-phase geometry optimization and measure the bond lengths and angles in the optimized complexes. Calculations were accomplished with the basis set/functional pairing of unrestricted dispersion-corrected B3LYP-d3[55−58] and basis set lacvp** for nonmetals C, H, N, O, S, and F along with basis set lacv3p** for Mn.[59,60] Successful ground-state optimizations were assessed by the forces on the all atoms residing below 10^{-5} hartrees/bohr as well as total energy remaining unchanged by 10^{-4} between the final SCF iterations. Oxidation states of clusters **oxCa′**, **oxCa′′**, **redCa′**, and **redCa′′** were tabulated through Mullikan spin populations and inspection of the spin-density plots. For structure **redCa′′**, wave functions with (**redCa′′**) and without (**redCa′′-noH**) hydrogen bonding between triflate and the hydroxide motif were isolated.

■ ASSOCIATED CONTENT

Supporting Information

The Supporting Information is available free of charge on the ACS Publications website at DOI: 10.1021/acs.inorgchem.8b02701.

Experimental procedures, NMR spectra, computational details, EPR spectra, and X-ray crystallographic data (PDF)

Accession Codes

CCDC 1035166 and 1035222 contain the supplementary crystallographic data for this paper. These data can be obtained free of charge via www.ccdc.cam.ac.uk/data_request/cif, or by emailing data_request@ccdc.cam.ac.uk, or by contacting The Cambridge Crystallographic Data Centre, 12 Union Road, Cambridge CB2 1EZ, UK; fax: +44 1223 336033.

■ AUTHOR INFORMATION

Corresponding Author

*E-mail: agapie@caltech.edu.

ORCID

Davide Lionetti: 0000-0002-4937-886X
Kurtis M. Carsch: 0000-0003-4432-7518
William A. Goddard, III: 0000-0003-0097-5716
R. David Britt: 0000-0003-0889-8436
Theodor Agapie: 0000-0002-9692-7614

Notes

The authors declare no competing financial interest.

■ ACKNOWLEDGMENTS

This work was supported by the California Institute of Technology and the NIH R01 GM102687A (T.A.). T.A. is a Dreyfus fellow. We thank Dr. Michael K. Takase and Lawrence M. Henling for assistance with X-ray crystallography. D.L. gratefully acknowledges a graduate fellowship from the Resnick Sustainability Institute at Caltech. K.C. and W.A.G. received support from the NSF (CBET-1512759). The Bruker KAPPA APEXII X-ray diffractometer was purchased via an NSF Chemistry Research Instrumentation award to Caltech (CHE-0639094). Computational resources included the Extreme Science and Engineering Discovery Environment, which is supported by National Science Foundation Grant ACI-1548562.

■ REFERENCES

(1) Fukuzumi, S. *Prog. Inorg. Chem.* **2009**, *56*, 49−154.
(2) Fukuzumi, S.; Ohkubo, K. Metal ion-coupled and decoupled electron transfer. *Coord. Chem. Rev.* **2010**, *254*, 372−385.
(3) Tsui, E. Y.; Kanady, J. S.; Agapie, T. Synthetic Cluster Models of Biological and Heterogeneous Manganese Catalysts for O-2 Evolution. *Inorg. Chem.* **2013**, *52*, 13833−13848.
(4) Umena, Y.; Kawakami, K.; Shen, J. R.; Kamiya, N. Crystal structure of oxygen-evolving photosystem II at a resolution of 1 9 angstrom. *Nature* **2011**, *473*, 55−U65.
(5) Yano, J.; Yachandra, V. Mn_4Ca Cluster in Photosynthesis: Where and How Water is Oxidized to Dioxygen. *Chem. Rev.* **2014**, *114*, 4175−4205.
(6) Suntivich, J.; Gasteiger, H. A.; Yabuuchi, N.; Nakanishi, H.; Goodenough, J. B.; Shao-Horn, Y. Design principles for oxygen-reduction activity on perovskite oxide catalysts for fuel cells and metal-air batteries (vol 3, pg 546, 2011). *Nat. Chem.* **2011**, *3*, 647−647.
(7) Suntivich, J.; May, K. J.; Gasteiger, H. A.; Goodenough, J. B.; Shao-Horn, Y. A Perovskite Oxide Optimized for Oxygen Evolution Catalysis from Molecular Orbital Principles. *Science* **2011**, *334*, 1383−1385.
(8) Zaharieva, I.; Najafpour, M. M.; Wiechen, M.; Haumann, M.; Kurz, P.; Dau, H. Synthetic manganese-calcium oxides mimic the water-oxidizing complex of photosynthesis functionally and structurally. *Energy Environ. Sci.* **2011**, *4*, 2400−2408.
(9) Lau, T. C.; Mak, C. K. Oxidation of Alkanes by Barium Ruthenate in Acetic-Acid - Catalysis by Lewis-Acids. *J. Chem. Soc., Chem. Commun.* **1993**, 766−767.
(10) Lau, T. C.; Wu, Z. B.; Bai, Z. L.; Mak, C. K. Lewis-Acid Catalyzed Oxidation of Alkanes by Chromate and Permanganate. *J. Chem. Soc., Dalton Trans.* **1995**, 695−696.
(11) Ho, C. M.; Lau, T. C. Lewis acid activated oxidation of alkanes by barium ferrate. *New J. Chem.* **2000**, *24*, 587−590.
(12) Lai, S.; Lee, D. G. Lewis acid assisted permanganate oxidations. *Tetrahedron* **2002**, *58*, 9879−9887.
(13) Yiu, S. M.; Wu, Z. B.; Mak, C. K.; Lau, T. C. FeCl3-activated oxidation of alkanes by [Os(N)O3] (−). *J. Am. Chem. Soc.* **2004**, *126*, 14921−14929.
(14) Yiu, S. M.; Man, W. L.; Lau, T. C. Efficient catalytic oxidation of alkanes by lewis acid/[Os-VI(N)CI4](−) using peroxides as terminal oxidants. Evidence for a metal-based active intermediate. *J. Am. Chem. Soc.* **2008**, *130*, 10821−10827.
(15) Du, H. X.; Lo, P. K.; Hu, Z. M.; Liang, H. J.; Lau, K. C.; Wang, Y. N.; Lam, W. W. Y.; Lau, T. C. Lewis acid-activated oxidation of alcohols by permanganate. *Chem. Commun.* **2011**, *47*, 7143−7145.
(16) Miller, C. G.; Gordon-Wylie, S. W.; Horwitz, C. P.; Strazisar, S. A.; Peraino, D. K.; Clark, G. R.; Weintraub, S. T.; Collins, T. J. A method for driving O-atom transfer: Secondary ion binding to a tetraamide macrocyclic ligand. *J. Am. Chem. Soc.* **1998**, *120*, 11540−11541.
(17) Fukuzumi, S.; Morimoto, Y.; Kotani, H.; Naumov, P.; Lee, Y. M.; Nam, W. Crystal structure of a metal ion-bound oxoiron(IV) complex and implications for biological electron transfer. *Nat. Chem.* **2010**, *2*, 756−759.

DOI: 10.1021/acs.inorgchem.8b02701
Inorg. Chem. XXXX, XXX, XXX−XXX

(18) Morimoto, Y.; Kotani, H.; Park, J.; Lee, Y. M.; Nam, W.; Fukuzumi, S. Metal Ion-Coupled Electron, Transfer of a Nonheme Oxoiron(IV) Complex: Remarkable Enhancement of Electron-Transfer Rates by Sc3+. *J. Am. Chem. Soc.* **2011**, *133*, 403−405.
(19) Park, J.; Morimoto, Y.; Lee, Y. M.; Nam, W.; Fukuzumi, S. Metal Ion Effect on the Switch of Mechanism from Direct Oxygen Transfer to Metal Ion-Coupled Electron Transfer in the Sulfoxidation of Thioanisoles by a Non-Heme Iron(IV)-Oxo Complex. *J. Am. Chem. Soc.* **2011**, *133*, 5236−5239.
(20) Lee, Y. M.; Bang, S.; Kim, Y. M.; Cho, J.; Hong, S.; Nomura, T.; Ogura, T.; Troeppner, O.; Ivanovic-Burmazovic, I.; Sarangi, R.; Fukuzumi, S.; Nam, W. A mononuclear nonheme iron(III)-peroxo complex binding redox-inactive metal ions. *Chem. Sci.* **2013**, *4*, 3917−3923.
(21) Yoon, H.; Lee, Y. M.; Wu, X.; Cho, K. B.; Sarangi, R.; Nam, W.; Fukuzumi, S. Enhanced Electron-Transfer Reactivity of Nonheme Manganese(IV)-Oxo Complexes by Binding Scandium Ions. *J. Am. Chem. Soc.* **2013**, *135*, 9186−9194.
(22) Nam, W.; Lee, Y. M.; Fukuzumi, S. Tuning Reactivity and Mechanism in Oxidation Reactions by Mononuclear Nonheme Iron(IV)-Oxo Complexes. *Acc. Chem. Res.* **2014**, *47*, 1146−1154.
(23) Park, J.; Morimoto, Y.; Lee, Y. M.; Nam, W.; Fukuzumi, S. Unified View of Oxidative C-H Bond Cleavage and Sulfoxidation by a Nonheme Iron(IV)-Oxo Complex via Lewis Acid-Promoted Electron Transfer. *Inorg. Chem.* **2014**, *53*, 3618−3628.
(24) Hong, S.; Pfaff, F. F.; Kwon, E.; Wang, Y.; Seo, M. S.; Bill, E.; Ray, K.; Nam, W. Spectroscopic Capture and Reactivity of a Low-Spin Cobalt(IV)-Oxo Complex Stabilized by Binding Redox-Inactive Metal Ions. *Angew. Chem., Int. Ed.* **2014**, *53*, 10403−10407.
(25) Hong, S.; Lee, Y. M.; Sankaralingam, M.; Vardhaman, A. K.; Park, Y. J.; Cho, K. B.; Ogura, T.; Sarangi, R.; Fukuzumi, S.; Nam, W. A Manganese(V)-Oxo Complex: Synthesis by Dioxygen Activation and Enhancement of Its Oxidizing Power by Binding Scandium Ion. *J. Am. Chem. Soc.* **2016**, *138*, 8523−8532.
(26) Bang, S.; Lee, Y. M.; Hong, S.; Cho, K. B.; Nishida, Y.; Seo, M. S.; Sarangi, R.; Fukuzumi, S.; Nam, W. Redox-inactive metal ions modulate the reactivity and oxygen release of mononuclear non-haem iron(III)-peroxo complexes. *Nat. Chem.* **2014**, *6*, 934−940.
(27) Lionetti, D.; Agapie, T. How calcium affects oxygen formation. *Nature* **2014**, *513*, 495−496.
(28) Dong, L.; Wang, Y. J.; Lv, Y. Z.; Chen, Z. Q.; Mei, F. M.; Xiong, H.; Yin, G. C. Lewis-Acid-Promoted Stoichiometric and Catalytic Oxidations by Manganese Complexes Having Cross-Bridged Cyclam Ligand: A Comprehensive Study. *Inorg. Chem.* **2013**, *52*, 5418−5427.
(29) Zhang, Z.; Coats, K. L.; Chen, Z.; Hubin, T. J.; Yin, G. Influence of Calcium(II) and Chloride on the Oxidative Reactivity of a Manganese(II) Complex of a Cross-Bridged Cyclen Ligand. *Inorg. Chem.* **2014**, *53*, 11937−11947.
(30) Chen, Z.; Yang, L.; Choe, C.; Lv, Z.; Yin, G. Non-redox metal ion promoted oxygen transfer by a non-heme manganese catalyst. *Chem. Commun.* **2015**, *51*, 1874−1877.
(31) Zhang, J.; Wang, Y.; Luo, N.; Chen, Z.; Wu, K.; Yin, G. Redox inactive metal ion triggered N-dealkylation by an iron catalyst with dioxygen activation: a lesson from lipoxygenases. *Dalton Trans.* **2015**, *44*, 9847−9859.
(32) Zhang, J.; Wei, W.-J.; Lu, X.; Yang, H.; Chen, Z.; Liao, R.-Z.; Yin, G. Nonredox Metal Ions Promoted Olefin Epoxidation by Iron(II) Complexes with H2O2: DFT Calculations Reveal Multiple Channels for Oxygen Transfer. *Inorg. Chem.* **2017**, *56*, 15138−15149.
(33) Zhang, J.; Yang, H.; Sun, T.; Chen, Z.; Yin, G. Nonredox Metal-Ions-Enhanced Dioxygen Activation by Oxidovanadium(IV) Complexes toward Hydrogen Atom Abstraction. *Inorg. Chem.* **2017**, *56*, 834−844.
(34) Li, F. F.; Van Heuvelen, K. M.; Meier, K. K.; Munck, E.; Que, L. Sc3+-Triggered Oxoiron(IV) Formation from O-2 and its Non-Heme Iron(II) Precursor via a Sc3+-Peroxo-Fe3+ Intermediate. *J. Am. Chem. Soc.* **2013**, *135*, 10198−10201.
(35) Kal, S.; Draksharapu, A.; Que, L. Sc3+ (or HClO4) Activation of a Nonheme FeIII−OOH Intermediate for the Rapid Hydroxylation of Cyclohexane and Benzene. *J. Am. Chem. Soc.* **2018**, *140*, 5798−5804.
(36) Prakash, J.; Rohde, G. T.; Meier, K. K.; Jasniewski, A. J.; Van Heuvelen, K. M.; Munck, E.; Que, L. Spectroscopic Identification of an Fe-III Center, not Fe-IV, in the Crystalline Sc-O-Fe Adduct Derived from [Fe-IV(O)(TMC)](2+). *J. Am. Chem. Soc.* **2015**, *137*, 3478−3481.
(37) Swart, M. A change in the oxidation state of iron: scandium is not innocent. *Chem. Commun.* **2013**, *49*, 6650−6652.
(38) Prakash, J.; Rohde, G. T.; Meier, K. K.; Jasniewski, A. J.; Van Heuvelen, K. M.; Munck, E.; Que, L. Spectroscopic Identification of an FeIII Center, not FeIV, in the Crystalline Sc-O-Fe Adduct Derived from [Fe(IV)(O)(TMC)]2+. *J. Am. Chem. Soc.* **2015**, *137*, 3478−3481.
(39) Lin, P. H.; Takase, M. K.; Agapie, T. Investigations of the Effect of the Non-Manganese Metal in Heterometallic-Oxido Cluster Models of the Oxygen Evolving Complex of Photosystem II: Lanthanides as Substitutes for Calcium. *Inorg. Chem.* **2015**, *54*, 59−64.
(40) Tsui, E. Y.; Agapie, T. Reduction potentials of heterometallic manganese-oxido cubane complexes modulated by redox-inactive metals. *Proc. Natl. Acad. Sci. U. S. A.* **2013**, *110*, 10084−10088.
(41) Kanady, J. S.; Tsui, E. Y.; Day, M. W.; Agapie, T. A Synthetic Model of the Mn3Ca Subsite of the Oxygen-Evolving Complex in Photosystem II. *Science* **2011**, *333*, 733−736.
(42) Herbert, D. E.; Lionetti, D.; Rittle, J.; Agapie, T. Heterometallic Triiron-Oxo/Hydroxo Clusters: Effect of Redox-Inactive Metals. *J. Am. Chem. Soc.* **2013**, *135*, 19075−19078.
(43) Tsui, E. Y.; Tran, R.; Yano, J.; Agapie, T. Redox-inactive metals modulate the reduction potential in heterometallic manganese-oxido clusters. *Nat. Chem.* **2013**, *5*, 293−299.
(44) Chantarojsiri, T.; Ziller, J. W.; Yang, J. Y. Incorporation of redox-inactive cations promotes iron catalyzed aerobic C-H oxidation at mild potentials. *Chem. Sci.* **2018**, *9*, 2567−2574.
(45) Reath, A. H.; Ziller, J. W.; Tsay, C.; Ryan, A. J.; Yang, J. Y. Redox Potential and Electronic Structure Effects of Proximal Nonredox Active Cations in Cobalt Schiff Base Complexes. *Inorg. Chem.* **2017**, *56*, 3713−3718.
(46) Duan, P.-C.; Manz, D.-H.; Dechert, S.; Demeshko, S.; Meyer, F. Reductive O2 Binding at a Dihydride Complex Leading to Redox Interconvertible μ-1,2-Peroxo and μ-1,2-Superoxo Dinickel(II) Intermediates. *J. Am. Chem. Soc.* **2018**, *140*, 4929−4939.
(47) Kumar, A.; Lionetti, D.; Day, V. W.; Blakemore, J. D. Trivalent Lewis Acidic Cations Govern the Electronic Properties and Stability of Heterobimetallic Complexes of Nickel. *Chem. - Eur. J.* **2018**, *24*, 141−149.
(48) Chantarojsiri, T.; Reath, A. H.; Yang, J. Cationic Charges Lead to Inverse Free Energy Relationship for N—N Bond Formation by Mn(VI) Nitrides. *Angew. Chem., Int. Ed.* **2018**, *57*, 14037.
(49) Evangelisti, F.; Moré, R.; Hodel, F.; Luber, S.; Patzke, G. R. 3d−4f {CoII3Ln(OR)4} Cubanes as Bio-Inspired Water Oxidation Catalysts. *J. Am. Chem. Soc.* **2015**, *137*, 11076−11084.
(50) Kanady, J. S.; Mendoza-Cortes, J. L.; Tsui, E. Y.; Nielsen, R. J.; Goddard, W. A.; Agapie, T. Oxygen Atom Transfer and Oxidative Water Incorporation in Cuboidal Mn3MOn, Complexes Based on Synthetic, Isotopic Labeling and Computational Studies. *J. Am. Chem. Soc.* **2013**, *135*, 1073−1082.
(51) Perrin, D. D. *International Union of Pure and Applied Chemistry, Commission on Equilibrium Data: Ionisation Constants of Inorganic Acids and Bases in Aqueous Solution*, 2nd ed.; Pergamon Press: Oxford Oxfordshire ; New York, 1982; p xiii.
(52) Tsui, E. Y.; Kanady, J. S.; Day, M. W.; Agapie, T. Trinuclear first row transition metal complexes of a hexapyridyl, trialkoxy 1,3,5-triarylbenzene ligand. *Chem. Commun.* **2011**, *47*, 4189−4191.
(53) Xu, A.; Xiong, H.; Yin, G. Distinct Oxygenation Difference between Manganese(IV) Hydroxo and Oxo Moieties: Electron Transfer versus Concerted Oxygen Transfer. *Chem. - Eur. J.* **2009**, *15*, 11478−11481.

DOI: 10.1021/acs.inorgchem.8b02701
Inorg. Chem. XXXX, XXX, XXX−XXX

(54) Bochevarov, A. D.; Harder, E.; Hughes, T. F.; Greenwood, J. R.; Braden, D. A.; Philipp, D. M.; Rinaldo, D.; Halls, M. D.; Zhang, J.; Friesner, R. A. Jaguar: A high-performance quantum chemistry software program with strengths in life and materials sciences. *Int. J. Quantum Chem.* **2013**, *113*, 2110−2142.
(55) Becke, A. D. Density-functional thermochemistry. III. The role of exact exchange. *J. Chem. Phys.* **1993**, *98*, 5648−5652.
(56) Becke, A. D. Density-functional exchange-energy approximation with correct asymptotic behavior. *Phys. Rev. A: At., Mol., Opt. Phys.* **1988**, *38*, 3098−3100.
(57) Lee, C. T.; Yang, W. T.; Parr, R. G. Development of the Colle-Salvetti Correlation-Energy Formula into a Functional of the Electron-Density. *Phys. Rev. B: Condens. Matter Mater. Phys.* **1988**, *37*, 785−789.
(58) Grimme, S. Semiempirical hybrid density functional with perturbative second-order correlation. *J. Chem. Phys.* **2006**, *124*, No. 034108.
(59) Francl, M. M.; Pietro, W. J.; Hehre, W. J.; Binkley, J. S.; Gordon, M. S.; DeFrees, D. J.; Pople, J. A. Self-consistent molecular orbital methods. XXIII. A polarization-type basis set for second-row elements. *J. Chem. Phys.* **1982**, *77*, 3654−3665.
(60) Hehre, W. J.; Ditchfield, R.; Pople, J. A. Self—Consistent Molecular Orbital Methods. XII. Further Extensions of Gaussian—Type Basis Sets for Use in Molecular Orbital Studies of Organic Molecules. *J. Chem. Phys.* **1972**, *56*, 2257−2261.

DOI: 10.1021/acs.inorgchem.8b02701
Inorg. Chem. XXXX, XXX, XXX−XXX